

contribute to the transport of heat. However, we consider both the translational and the torsional vibrations of the rigid molecules. This leads to the factor of 2 in Eq. 2. With all quantities in Eq. 2 known, we can calculate  $\Lambda_{\text{Eins}}$  (dashed curve in Fig. 4). The agreement between theory and experiment from 300 to 10 K, achieved without any adjustable parameters, is taken as evidence that we correctly identified the excitations in the specific heat measurements and also the mechanism of the heat transport. The transition from torsional vibration to nearly free rotation expected to occur at  $\sim 250$  K does not appear to have a noticeable effect. The excitations that dominate the specific heat above  $\sim 40$  K (by as much as an order of magnitude at 300 K) do not appear to contribute to the heat flow at all, which means that they are truly localized.

Einstein's theory of thermal conductivity quite obviously fails below  $\sim 10$  K [as it does in all amorphous solids as well (5)]. In this temperature range collective excitations become noticeable in specific heat, and they should contribute to the heat flow, thus increasing the thermal conductivity. As shown in Fig. 5, the thermal conductivity of the  $C_{60}/C_{70}$  compacts is similar in this temperature range to that observed in all amorphous solids, in which the phonon scattering by the low-energy [tunneling (25)] excitations leads to a thermal conductivity that varies as  $T^2$ . (Some additional grain boundary scattering appears to occur in the compacts, which decreases the conductivity at the lowest temperatures. Diffuse scattering with a mean free path of  $\sim 20$   $\mu\text{m}$  may be responsible for this effect.) Because both thermal conductivity and low-temperature specific heat of the compacts are similar to those of amorphous solids, we do not believe that some accidental random impurities are the cause. The origin of the glasslike excitations, which are obviously absent in the single-crystal  $C_{60}$  (see the thermal conductivity data in Fig. 4) are as yet unexplained. The point to be stressed here is the observation of a solid with lattice vibrations that are described by the Einstein localized oscillator model over a wide frequency range much better than by the standard Debye model, which is based on plane waves.

## REFERENCES AND NOTES

1. A. Einstein, *Ann Phys.* **22**, 180 (1907).
2. ———, *ibid.* **35**, 679 (1911); the essential part of this paper is reproduced in English in (6).
3. P. Debye, *ibid.* **39**, 789 (1912).
4. M. Born and Th. von Karman, *Phys. Z.* **13**, 297 (1912).
5. D. G. Cahill and R. O. Pohl, *Solid State Commun.* **70**, 927 (1989).
6. D. G. Cahill, S. K. Watson, R. O. Pohl, *Phys. Rev. B* **46**, 6131 (1992).
7. M. Meissner, A. Tausend, D. Wobig, *Phys. Status Solidi A* **49**, 59 (1978).
8. From Texas Fullerenes Corporation, Houston, TX 77002.
9. A. MacKay *et al.*, unpublished results as quoted in H. W. Kroto, A. W. Allaf, S. P. Balm, *Chem. Rev.* **91**, 1213 (1991), reference 237.
10. K. A. Topp, work in progress.
11. D. G. Cahill, H. E. Fischer, S. K. Watson, R. O. Pohl, G. A. Slack, *Phys. Rev. B* **40**, 3254 (1989).
12. N. D. Birge and S. R. Nagel, *Rev. Sci. Instrum.* **58**, 1464 (1987).
13. D. G. Cahill, *ibid.* **61**, 802 (1990).
14. Y. S. Touloukian and E. H. Buyco, Eds., *Specific Heat of Nonmetallic Solids, Thermophysical Data Series* (IFI/Plenum, New York, 1970).
15. M. G. Alexander, D. P. Goshorn, D. G. Onn, *Phys. Rev. B* **22**, 4535 (1980).
16. J. A. Krumhansl and H. Brooks, *J. Chem. Phys.* **21**, 1663 (1952); B. J. C. van der Hoeven, Jr., and P. H. Keesom, *Phys. Rev.* **130**, 1318 (1963).
17. T. Atake *et al.*, *Physica C* **185–189**, 427 (1991), see also T. Matsuo *et al.*, *Solid State Commun.* **83**, 711 (1992).
18. P. A. Heiney *et al.*, *Phys. Rev. Lett.* **66**, 2911 (1991); R. Sachidanandam and A. B. Harris, *ibid.* **67**, 1467 (1991); W. I. F. David *et al.*, *Nature* **353**, 147 (1991); R. D. Johnson, C. S. Yannoni, H. C. Dorn, J. R. Salem, D. S. Bethune, *Science* **255**, 1235 (1992).
19. D. A. Neumann *et al.*, *J. Chem. Phys.* **96**, 8631 (1992).
20. W. P. Beyermann, M. F. Hundley, J. D. Thompson, F. N. Diederich, G. Gruner, *Phys. Rev. Lett.* **68**, 2046 (1992). A sizable linear anomaly above 1.4 K reported in that paper has since been found to be a materials-synthesis artifact due to an organic solvent used in the process (M. F. Hundley, personal communication).
21. R. E. Stanton and N. D. Newton, *J. Phys. Chem.* **92**, 2141 (1988); D. E. Weeks and W. G. Harter, *Chem. Phys. Lett.* **144**, 3666 (1988). For a recent critical review of calculated normal modes, see F. Negri, G. Orlandi, F. Zerbetto, *J. Am. Chem. Soc.* **113**, 6037 (1991).
22. Amorphous  $\text{SiO}_2$ , see (3) for  $T < 1$ , and J. R. Olson, H. E. Fischer, and R. O. Pohl [*J. Am. Ceram. Soc.* **74**, 564 (1991)] for a collection of references for  $T > 1$  K Polystyrene R. B. Stephens [thesis, Cornell University (1974) (available as Cornell Materials Science Center Rep 2304)] ( $T < 1$  K) and R. B. Stephens, G. S. Cieloszyk, and G. L. Salinger [*Phys. Lett. A* **38**, 215 (1972)] ( $T < 0.5$  K); see B. Wunderlich and H. Baur, *Adv. Polym. Sci.* **7**, 151 (1970); see p. 314 for a summary of measurements for  $T > 1$  K.
23. R. O. Pohl, in *Amorphous Solids, Low Temperature Properties*, W. A. Phillips, Ed. (vol. 24 of Topics in Current Physics, Springer-Verlag, Berlin, 1981), pp. 27–50.
24. P. W. Anderson, B. I. Halpern, C. M. Varma, *Philos. Mag.* **25**, 1 (1972); W. A. Phillips, *J. Low Temp. Phys.* **7**, 351 (1972); *Rep. Progr. Phys.* **50**, 1657 (1987).
25. S. Hoen *et al.*, *Phys. Rev. B* **46**, 12737 (1992).
26. A. K. Raychaudhuri, unpublished results.
27. X. D. Shi *et al.*, *Phys. Rev. Lett.* **68**, 827 (1992).
28. T. Klitsner and R. O. Pohl, *Phys. Rev. B* **36**, 6551 (1987), see p. 6554.
29. R. Berman, P. R. W. Hudson, M. Martinez, *J. Phys. C* **8**, L430 (1975).
30. R. C. Yu, N. Tea, M. B. Salamon, D. Lorents, R. Malhotra, *Phys. Rev. Lett.* **68**, 2050 (1992).
31. T. Nihira and T. Iwata, *Jpn. J. Appl. Phys.* **14**, 1099 (1975); D. T. Morelli and C. Uher, *Phys. Rev. B* **31**, 6721 (1985).
32. D. G. Cahill and R. O. Pohl, *Annu. Rev. Phys. Chem.* **39**, 93 (1988).
33. We thank N. W. Ashcroft, M. Meissner, A. K. Raychaudhuri, M. D. Hornbostel, and S. A. Fitzgerald for illuminating discussions and for help with the experiments. Supported by National Science Foundation grant DMR-91-15981 and the Cornell Materials Science Center.

1 October 1992, accepted 11 December 1992

## Mid-Depth Circulation of the Subpolar North Atlantic During the Last Glacial Maximum

D. W. Oppo\* and S. J. Lehman

Holocene and glacial carbon isotope data of benthic foraminifera from shallow to mid-depth cores from the northeastern subpolar Atlantic show that this region was strongly stratified, with carbon-13-enriched glacial North Atlantic intermediate water (GNAIW) overlying carbon-13-depleted Southern Ocean water (SOW). The data suggest that GNAIW originated north of the polar front and define GNAIW end-member carbon isotope values for studies of water-mass mixing in the open Atlantic. Identical carbon isotope values in the core of GNAIW and below the subtropical thermocline are consistent with rapid cycling of GNAIW through the northern Atlantic. The high carbon isotope values below the thermocline indicate that enhanced nutrient leakage in response to increased ventilation may have extended into intermediate waters. Geochemical box models show that the atmospheric carbon dioxide response to nutrient leakage that results from an increase in ventilation rate may be greater than the response to nutrient redistribution by conversion of North Atlantic deep water into GNAIW. These results underscore the potential role of Atlantic Ocean circulation changes in influencing past atmospheric carbon dioxide values.

The general features of North Atlantic Ocean circulation during the last glaciation,  $\sim 18,000$  to 15,000 years ago, are fairly well understood, but several outstanding questions remain. Among these uncer-

tainties is the mode of formation and source region of high- $\delta^{13}\text{C}$  and low-Cd/Ca GNAIW as well as the origin of nutrient depletion in this water mass. Nutrient-poor (high  $\delta^{13}\text{C}$ , low Cd/Ca) lower North Atlantic deep water (NADW) now fills the deep northern and tropical Atlantic. During the last glaciation, this water mass was replaced by nutrient-rich SOW, whereas

Woods Hole Oceanographic Institution, Woods Hole, MA 02543

\*To whom correspondence should be addressed

**Table 1.** Core locations. Also given are mean  $\delta^{18}\text{O}$  and  $\delta^{13}\text{C}$  values ( $\pm$  numbers in parentheses represent the last two decimal values of the SD) for the Holocene and glacial data points circled in Fig. 3, A to E, and the change in  $\delta^{13}\text{C}$  values between the glacial and the Holocene.

Core	Location	Depth (m)	Holocene		Glacial		$\Delta\delta^{13}\text{C}$
			$\delta^{18}\text{O}$	$\delta^{13}\text{C}$	$\delta^{18}\text{O}$	$\delta^{13}\text{C}$	
V29-198	59°N 15°W	1139	2.29 (08)	1.07 (08)	3.77 (23)	1.54 (13)	0.47
V29-193	55°N 19°W	1326	2.32 (12)	1.29 (08)	3.85 (10)	1.52 (11)	0.23
V28-73	57°N 20°W	2063	2.77 (12)	1.17 (14)	4.14 (17)	1.16 (09)	0.01
CH73-139C (4)	55°N 16°W	2209	2.70 (04)	0.93 (04)	4.60 (14)	0.61 (16)	-0.32
V23-81 (7)	54°N 17°W	2393	2.29 (17)	0.94 (05)	4.19 (15)	0.45 (16)	-0.49

nutrient-depleted GNAIW filled the North Atlantic above about 2000 m (1-5). Geochemical box models of carbon cycling show a strong dependence of atmospheric  $\text{CO}_2$  on the mechanism of nutrient depletion in the upper ocean (6). For example, formation of GNAIW by the same high-latitude processes that ventilate the deep Atlantic today elicits a relatively weak alkalinity response and therefore has a relatively small impact on atmospheric  $\text{CO}_2$ . A larger atmospheric  $\text{CO}_2$  reduction can be produced by either an increase in the depth of nutrient regeneration or an increase in nutrient leakage to the deep ocean by more rapid ventilation of the thermocline (6).

In this report, we present Holocene and glacial  $\delta^{18}\text{O}$  and  $\delta^{13}\text{C}$  data of benthic foraminifera from three shallow to mid-depth

(1139 to 2063 m) cores on the Rockall Plateau in the subpolar North Atlantic (Table 1 and Fig. 1). Together with published results from deeper cores in the study area (4, 7) (Fig. 1), we used our data to reconstruct northern  $\delta^{13}\text{C}$  depth profiles (1139 to 2393 m) for the glacial ocean and to evaluate circulation of the glacial North Atlantic and its potential impact on atmospheric  $\text{CO}_2$ .

Lower NADW is now composed primarily of overflow waters from the Norwegian, Greenland, and Iceland seas that reach the Atlantic along several flow paths (8) (Fig. 1). These waters enter the northwestern Atlantic through the Denmark Strait, the Iceland Basin over the Iceland-Faroe Ridge and through the Faroe Bank Channel, and the Rockall Trough across the Wyville-Thompson Ridge. In addition, the deep northeastern Atlantic contains deep waters from the eastern Atlantic Basin to the south (eastern basin water) (9). The Rockall Plateau is located immediately downstream of overflows that cross the Wyville-Thompson Ridge and is within the influence of eastern basin water below 2000 m and of Labrador Sea water above this depth (10). More shallow depths of the northeastern Atlantic are influenced by Mediterranean Sea water that is high in salinity and low in  $\text{O}_2$  (10) and by subtropical waters that flow in from the southwest (9), some of which also appear to be depleted in  $\text{O}_2$ . The complex controls on surface-water  $\delta^{13}\text{C}$  and the dependence of  $\text{O}_2$  saturation on temperature result in decoupling of subsurface  $\delta^{13}\text{C}$  values from  $\text{O}_2$  concentration in water masses of different origin (Fig. 2).

We obtained isotope data of the benthic foraminifera *Cibicides wuellerstorfi* and *Cibicides kullenbergi* from the glacial-to-Holocene sections of cores V29-198, V29-193, and V28-73 [Tables 2 and 3 (14) and Fig. 3, A to C]. Large differences between the  $\delta^{18}\text{O}$  and  $\delta^{13}\text{C}$  values of *C. wuellerstorfi* and those of *C. kullenbergi* from the same depths are evident in core V29-198 (Table 2), but these differences are not evident in  $\delta^{18}\text{O}$ - $\delta^{13}\text{C}$  space. On the basis of the abundance of these two species relative to core depth (15), we suggest that the large isotope

differences are due to deep mixing of Holocene *C. kullenbergi* into the glacial section. Holocene foraminiferal  $\delta^{13}\text{C}$  values in our cores and in deeper cores from the same region (Fig. 3, D and E) are similar to modern  $\delta^{13}\text{C}$  measurements of total dissolved  $\text{CO}_2$  from a nearby Geochemical Ocean Sections Study (GEOSECS) station (Fig. 2), which confirms that both of these species closely record  $\delta^{13}\text{C}$  values of ambient deep water (16). Unlike the modern and Holocene data, glacial  $\delta^{13}\text{C}$  values show a marked gradient with depth. This gradient marks a boundary at  $\sim 2000$  m that separates shallow sites with  $\delta^{13}\text{C}$  values that are greater than those of the Holocene from deeper sites with  $\delta^{13}\text{C}$  values that are smaller than those of the Holocene (17).

The rapid  $\delta^{13}\text{C}$  decrease with depth indicates that the glacial water column was strongly stratified. The  $\delta^{13}\text{C}$  difference between 1139 and 2393 m increased from  $\sim 0.2$  per mil during the Holocene to  $\sim 1.0$  per mil during the last glaciation (Tables 2 and 3 and Fig. 2). During the Holocene, nutrient-depleted (high  $\delta^{13}\text{C}$ ) NADW was present over the Rockall Plateau to a depth of at least 2400 m (Fig. 2). By contrast, the large glacial  $\delta^{13}\text{C}$  gradient indicates that two distinct water masses were present: High- $\delta^{13}\text{C}$  GNAIW overlay a more nutrient-rich water mass of southern origin that was low in  $\delta^{13}\text{C}$ . The incursion of deep waters from the south is not surprising because the flow path of eastern basin water is now poised to exert a greater influence in the northeastern Atlantic if the contribution of dense overflows is reduced (Fig. 1). The high-latitude location and the high  $\delta^{13}\text{C}$  values measured in the shallow cores indicate that the core sites must lie in or near the core of GNAIW. These  $\delta^{13}\text{C}$  values can thus be treated as northern-source end-member values for the glacial ocean.

Above the depth of low-latitude sills

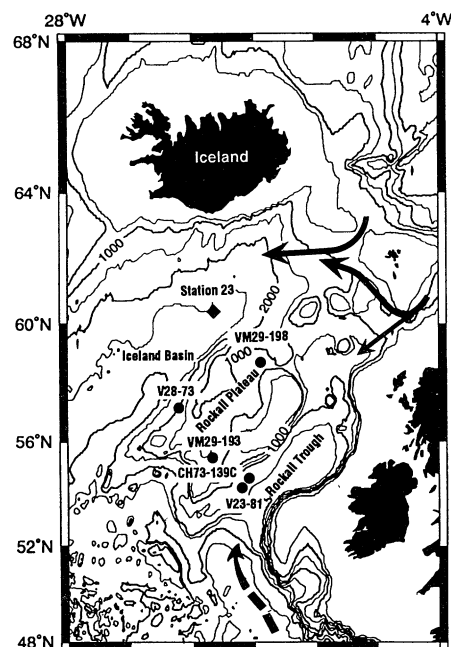


**Fig. 1.** Map of study area showing locations of cores and Geochemical Ocean Sections Study (GEOSECS) station 23 (60°N, 19°W). Also shown are the bottom currents that influence the region. Unbroken arrows denote overflow waters, and the broken arrow indicates eastern basin water. Depths indicated by thinner solid lines are in meters.

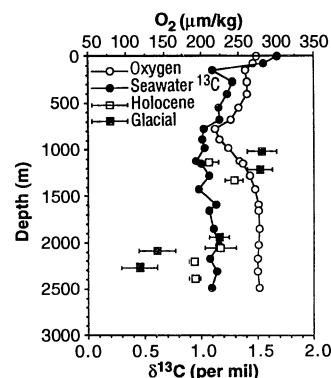


**Fig. 2.** Oxygen and  $\delta^{13}\text{C}$  profiles from GEOSECS station 23 (11, 12). Holocene and glacial benthic  $\delta^{13}\text{C}$  values (Tables 2 and 3) are also shown. The glacial data set is shifted upward by 120 m for correction of sea level (13).

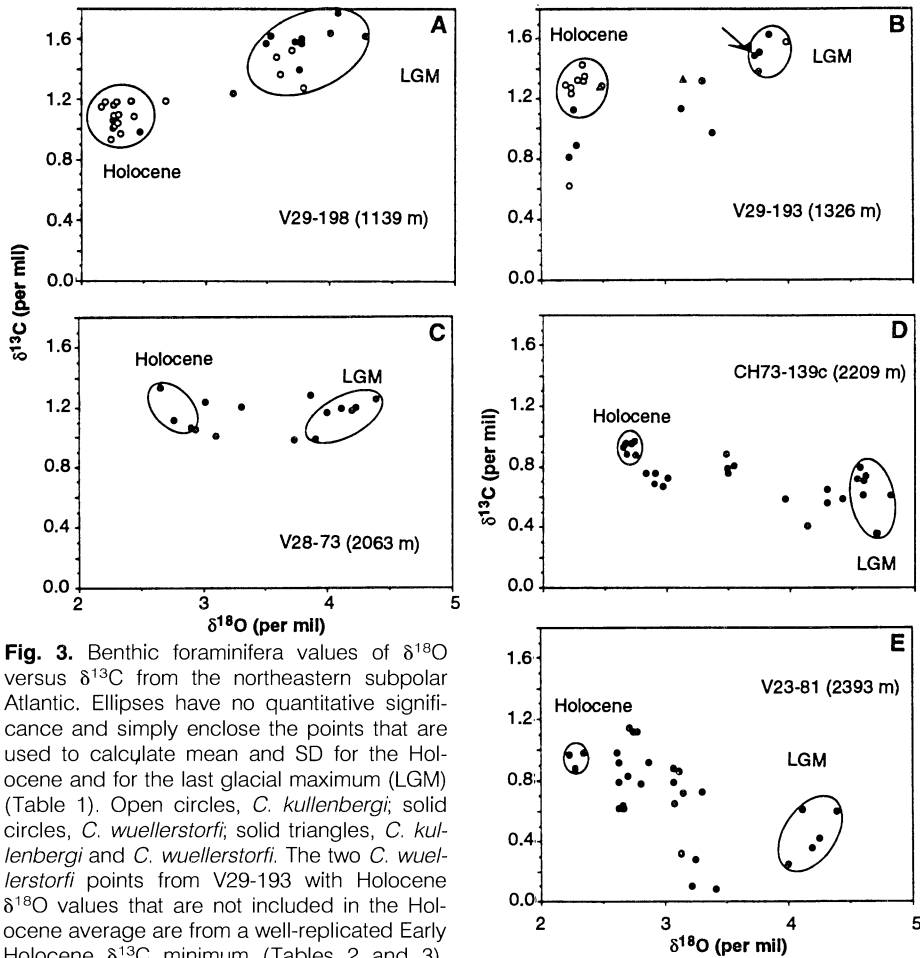


**Fig. 3.** Benthic foraminifera values of  $\delta^{18}\text{O}$  versus  $\delta^{13}\text{C}$  from the northeastern subpolar Atlantic. Ellipses have no quantitative significance and simply enclose the points that are used to calculate mean and SD for the Holocene and for the last glacial maximum (LGM) (Table 1). Open circles, *C. kullenbergi*; solid circles, *C. wuellerstorfi*; solid triangles, *C. kullenbergi* and *C. wuellerstorfi*. The two *C. wuellerstorfi* points from V29-193 with Holocene  $\delta^{18}\text{O}$  values that are not included in the Holocene average are from a well-replicated Early Holocene  $\delta^{13}\text{C}$  minimum (Tables 2 and 3). Because of the low sedimentation rates of the three more shallow cores, age and significance of the minimum are uncertain. The arrow in (B) indicates a point not included in the glacial average because it is associated with the deglaciation (Tables 2 and 3). Glacial  $\delta^{13}\text{C}$  values were higher than Holocene values in the shallow cores (A and B), approximately the same near 2000 m (C), and lower in the deeper cores (D and E).

(~3750 m) through which SOW and NADW now enter the eastern basin in a proportion of 1:4 (4) and below the depth that was influenced by GNAIW (~2000 m), glacial  $\delta^{13}\text{C}$  values in the eastern basin averaged 0.4 per mil in both tropical and subtropical regions (18, 19). With end-member  $\delta^{13}\text{C}$  values of 1.5 per mil for GNAIW (Table 1) and -0.85 per mil for SOW (20), we confirmed that equal parts of SOW and NADW entered the eastern basin during the last glaciation, as opposed to the proportion of 1:4 today (21, 22). Values of  $\delta^{13}\text{C}$  below the depth of the low-latitude sills were lower than those above the sills because of the long residence time of water within the deep basin (4, 18). Values that were measured in core V23-81 are close to the 0.4 per mil value measured near 5°N and 20°N above the sill depth in the eastern basin (18, 19) (Table 1). The similarity of these values suggests that water from above the depth of the low-latitude sills flowed northward with little input of low- $\delta^{13}\text{C}$  organic matter and filled the deep

northeastern Atlantic. Alternatively, whatever  $\delta^{13}\text{C}$  reduction occurred because of the addition of low- $\delta^{13}\text{C}$  organic matter as eastern basin water flowed northward was offset by a  $\delta^{13}\text{C}$  increase due to mixing with overlying high- $\delta^{13}\text{C}$  GNAIW. In either case, the low  $\delta^{13}\text{C}$  values of waters below 2000 m in the subpolar North Atlantic indicate that these waters are predominantly of southern origin.

Carbon isotope values from the shallow northeastern Atlantic are indistinguishable from those of Little Bahama Banks (23) in the western subtropical Atlantic (Fig. 4). The high  $\delta^{13}\text{C}$  values above 1000 m at Little Bahama Banks have been attributed to rapid ventilation of the thermocline and the accompanying increase in nutrient leakage from the thermocline into deeper waters, as was predicted by geochemical box-modeling studies (6, 23, 24). The absence of a  $\delta^{13}\text{C}$  gradient between the two sites (Fig. 4), which are separated by over 30° of latitude, may indicate that glacial productivity was low as a result of reduced

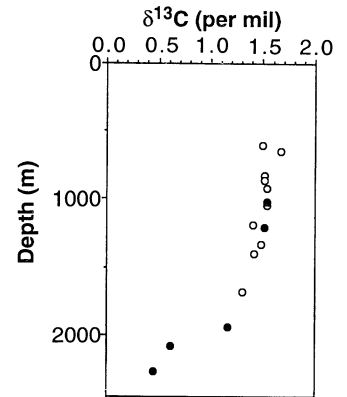


**Fig. 4.** Glacial  $\delta^{13}\text{C}$  values of benthic foraminifera from the northeastern subpolar Atlantic (solid circles) (Tables 2 and 3) and from Little Bahama Banks (open circles) (24). The deepest point in the Little Bahama Banks profile is from the Caribbean Sea (2, 5).

nutrient concentrations in the overlying surface and thermocline waters. However, modeling studies suggest that, despite the decrease in nutrient concentration, productivity increases as thermocline ventilation increases because the accompanying increase in low-latitude upwelling cycles nutrients to the surface more often (6, 24). In the models (and presumably in the glacial ocean), the upper ocean never becomes nutrient-free because some exchange of water continues between the model boxes. In this way, some fraction of the "leaked" nutrients is replenished and high productivity is sustained. A more likely explanation for the absence of a latitudinal  $\delta^{13}\text{C}$  gradient in intermediate waters is that the residence time of GNAIW in the North Atlantic was so short that the effect of productivity and remineralization of organic matter on GNAIW  $\delta^{13}\text{C}$  was negligible.

The high  $\delta^{13}\text{C}$  values (1.5 per mil) in the two more shallow cores confirm the absence of upwelled, low- $\delta^{13}\text{C}$  SOW in the subpolar Atlantic (25), which has been hypothesized in earlier studies (3, 26). High  $\delta^{13}\text{C}$  values in the mid-depth subpolar Atlantic are probably the result of several processes. First, the subtropical thermocline feed waters for GNAIW had high  $\delta^{13}\text{C}$  values (23). Second, if GNAIW also cycled rapidly, nutrient leakage that has been envisioned for the glacial thermocline (23, 24) may have extended deeper into intermediate depths, further increasing  $\delta^{13}\text{C}$  values. Third, if productivity increased, more low- $\delta^{13}\text{C}$  organic matter may have been regenerated in deeper waters, resulting in an additional increase in  $\delta^{13}\text{C}$  values in overlying GNAIW (6). Finally, GNAIW  $\delta^{13}\text{C}$  values were ~0.3 per mil higher than would be predicted on the basis of Cd/Ca data (27). If there was no decoupling between Cd and nutrients, the high

**Table 2.** Data for core V29-198 (Fig. 3A). Species coding is k = *C. kullenbergi*, w = *C. wuellerstorfi*, and c = mixed *C. kullenbergi* and *C. wuellerstorfi*. H indicates that the measurement was included in the Holocene mean and G denotes inclusion in the glacial mean (Table 1).

Depth (cm)	$\delta^{18}\text{O}$	$\delta^{13}\text{C}$	Species
0.5 <sup>H</sup>	2.260	1.163	k
2.5 <sup>H</sup>	2.278	1.051	k
6.5 <sup>H</sup>	2.163	1.151	k
10.0 <sup>H</sup>	2.258	1.060	k
15.0 <sup>H</sup>	2.295	1.038	k
21.0 <sup>H</sup>	2.265	1.089	k
25.0 <sup>H</sup>	2.298	1.097	k
30.0 <sup>H</sup>	2.272	1.020	k
30.0 <sup>H</sup>	2.315	0.973	k
35.0 <sup>H</sup>	2.401	1.185	k
35.0 <sup>H</sup>	2.255	1.009	k
40.0 <sup>H</sup>	2.242	0.933	k
50.0 <sup>H</sup>	2.472	0.982	w
60.0 <sup>G</sup>	3.760	1.399	w
60.0 <sup>G</sup>	3.774	1.572	w
65.0 <sup>H</sup>	2.285	1.178	k
65.0 <sup>H</sup>	2.192	1.183	k
65.0 <sup>G</sup>	4.067	1.775	w
65.0 <sup>G</sup>	4.285	1.624	w
72.0 <sup>H</sup>	2.422	1.082	k
72.0 <sup>*</sup>	2.676	1.189	k
72.0 <sup>G</sup>	3.770	1.601	w
72.0 <sup>†</sup>	3.223	1.240	w
72.0 <sup>G</sup>	3.487	1.573	w
75.0 <sup>G</sup>	4.006	1.643	w
80.0 <sup>G</sup>	3.607	1.363	k
80.0 <sup>G</sup>	3.530	1.620	w
80.0 <sup>G</sup>	3.716	1.584	w
85.0 <sup>G</sup>	3.696	1.527	k
90.0 <sup>G</sup>	3.786	1.274	k
90.0 <sup>G</sup>	3.572	1.480	k

\*Rejected because  $\delta^{18}\text{O}$  is a 2-SD outlier †Rejected because low values were not confirmed by two additional analyses.

**Table 3.** Data for cores V29-193 and V28-73 (Fig. 3, B and C). Abbreviations and symbols are as in Tables 1 and 2.

Depth (cm)	$\delta^{18}\text{O}$	$\delta^{13}\text{C}$	Species
V29-193			
0.5 <sup>H</sup>	2.253	1.229	k
0.5 <sup>H</sup>	2.305	1.322	k
3.0 <sup>H</sup>	2.350	1.426	k
5.0 <sup>H</sup>	2.353	1.314	k
5.0 <sup>H</sup>	2.207	1.287	k
10.0 <sup>H</sup>	2.252	1.270	k
15.0 <sup>H</sup>	2.502	1.280	k
15.0 <sup>H</sup>	2.270	1.123	w
20.0 <sup>H</sup>	2.364	1.348	k
20.0 <sup>*</sup>	2.234	0.617	k
25.0	2.294	0.888	w
25.0	2.228	0.810	w
31.5 <sup>H</sup>	2.487	1.278	c
35.0	3.737	1.485	w
35.0	3.144	1.132	w
45.0	3.155	1.325	c
55.0 <sup>G</sup>	3.769	1.376	w
60.0 <sup>G</sup>	3.853	1.625	w
64.5 <sup>†</sup>	3.386	0.970	w
64.5 <sup>G</sup>	3.776	1.505	w
70.0 <sup>G</sup>	3.986	1.575	k
70.0 <sup>†</sup>	3.314	1.315	w
V28-73			
3.5 <sup>H</sup>	2.652	1.333	w
10.0 <sup>H</sup>	2.899	1.068	w
15.0 <sup>H</sup>	2.765	1.119	w
20.0	3.019	1.240	w
25.0	3.099	1.011	w
25.0	3.312	1.209	w
30.0	2.938	1.056	w
35.0	3.733	0.986	w
43.0 <sup>G</sup>	4.391	1.259	w
50.0 <sup>G</sup>	4.226	1.202	w
55.0 <sup>G</sup>	3.907	0.988	w
60.0 <sup>G</sup>	4.201	1.178	w
64.0 <sup>G</sup>	4.113	1.196	w
64.0 <sup>G</sup>	4.001	1.165	w

\*Not included because  $\delta^{13}\text{C}$  is a 2-SD outlier †Rejected from mean because of low isotope values relative to those of other glacial points (Fig. 3B). Their inclusion would result in means of  $3.68 \pm 0.27$  ( $\delta^{18}\text{O}$ ) and  $1.39 \pm 0.24$  ( $\delta^{13}\text{C}$ ).

$\delta^{13}\text{C}$  values indicate that changes in the photosynthetic fractionation factor (28) or in thermodynamic processes (29) also influenced the  $^{13}\text{C}$  content of GNAIW.

The high- $\delta^{13}\text{C}$  waters over the shallow Rockall Plateau probably formed north of the glacial polar front. Relatively high benthic  $\delta^{13}\text{C}$  values (1.3 per mil) indicate that the deep Norwegian Sea was a possible source for GNAIW (30). A major source of this water in the subpolar Atlantic, however, is indicated by a glacial surface salinity reconstruction from planktonic  $\delta^{18}\text{O}$  data and faunally derived sea-surface temperature (31). Calculations of density from this data set further suggest that Norwegian Sea surface waters were not dense enough to produce GNAIW (25). However, the restricted seasonal (summer) growth of the high-latitude planktonic foraminifera *Neogloboquadrina pachyderma* (32) may limit their relevance in the assessment of deep-water source areas. These estimates are for summer, although convection most likely occurred in fall or winter, when surface cooling weakened the seasonal salinity

stratification. Our results that suggest that the North Atlantic (Fig. 4) may have been rapidly ventilated, taken together with evidence for only limited surface inflow into the Norwegian Sea (33) and the corollary of only limited outflow, also favor a significant subpolar source of GNAIW.

Our results indicate that the core of nutrient-depleted GNAIW, with  $\delta^{13}\text{C}$  values of  $\sim 1.5$  per mil, was located near a depth of 1000 m in the subpolar northeastern Atlantic, more shallow and farther north than previously documented. High  $\delta^{13}\text{C}$  values in the subtropical thermocline feed waters clearly played a role in the elevation of  $\delta^{13}\text{C}$  values in GNAIW. Evidence that GNAIW cycled rapidly through the North Atlantic suggests that the leakage into deeper waters of low- $\delta^{13}\text{C}$  organic matter also resulted in high GNAIW  $\delta^{13}\text{C}$  values. The associated increase in low-latitude upwelling and productivity may

have caused more organic matter to be regenerated at depth, further increasing the  $\delta^{13}\text{C}$  value of GNAIW. Box models suggest that an increase either in nutrient leakage to the deep ocean or in the fraction of organic matter that is regenerated in the deep ocean can decrease atmospheric  $\text{CO}_2$  levels more effectively than by the shoaling of NADW to form GNAIW. The observations presented here lend additional support to hypotheses that implicate changes in North Atlantic circulation as a major source of past atmospheric  $\text{CO}_2$  variations (8, 24).

REFERENCES AND NOTES

1. E. A. Boyle and L. D. Keigwin, *Science* **218**, 784 (1982).
2. D. W. Oppo and R. G. Fairbanks [*Earth Planet. Sci. Lett.* **86**, 1 (1987)] suggest that the Mediterranean Sea may have been a source of GNAIW, but Ba/Ca data indicate that its contribution must have been minimal [D. W. Lea and E. A. Boyle, *Paleoceanography* **5**, 719 (1990)].
3. J. C. Duplessy et al., *Paleoceanography* **3**, 343 (1988).
4. W. B. Curry, J. C. Duplessy, L. D. Labeyrie, N. J. Shackleton, *ibid.*, p. 317
5. E. A. Boyle and L. Keigwin, *Nature* **330**, 35 (1987).
6. E. A. Boyle, *J. Geophys. Res.* **93**, 15701 (1988).
7. E. Jansen and T. Veum, *Nature* **343**, 612 (1990).
8. L. V. Worthington, *Johns Hopkins Oceanographic Studies* (Johns Hopkins Univ. Press, Baltimore, MD, 1976), vol. 6
9. W. J. Schmitz and M. S. McCartney, *Rev. Geophys.*, in press.
10. D. J. Ellett and J. H. A. Martin, *Deep Sea Res.* **20**, 585 (1973), J. Reid, *ibid.* **26**, 1199 (1979).
11. A. E. Bainbridge, *GEOSecs Atlantic Expedition 1* (National Science Foundation, Washington, DC, 1981).
12. P. Kroppnick, *Deep Sea Res.* **32**, 57 (1985).
13. R. G. Fairbanks, *Nature* **342**, 637 (1989).
14. Foraminifera were hand-picked from the size fraction that was  $>150 \mu\text{m}$  and were heated under a vacuum at  $375^\circ\text{C}$ . Samples typically containing about five foraminifera were reacted in a common acid bath (100% phosphoric acid) at  $90^\circ\text{C}$  and  $\text{CO}_2$  was manually extracted on line. The  $\text{CO}_2$  samples were introduced to a VG 903 Isogas mass spectrometer (VG Instruments) with a stable isotope ratio analysis source. The SD of standards during the measurement of these samples was 0.08 per mil for  $\delta^{18}\text{O}$  [ $\delta^{18}\text{O} = (^{18}\text{O}/^{16}\text{O})_{\text{sample}} \div (^{18}\text{O}/^{16}\text{O})_{\text{standard}} - 1$ ] 1000 per mil] and 0.05 per mil for  $\delta^{13}\text{C}$  [ $\delta^{13}\text{C} = (^{13}\text{C}/^{12}\text{C})_{\text{sample}} \div (^{13}\text{C}/^{12}\text{C})_{\text{standard}} - 1$ ] 1000 per mil]
15. The following are the values for the number of specimens per gram of sediment for depths in V29-198 that correspond to those in Table 1 for *C. wuellerstorfi*: 0.0, 0.0, 0.0, 0.0, 0.0, 0.0, 0.0, 0.2, 0.4, 0.2, 0.6, 0.0, 1.3, 0.9, 1.3, 0.9, 0.9, 0.7, 0.7, 0.3, 0.7, 0.2; and for *C. kullenbergi*: 1.2, 2.8, 2.8, 1.7, 4.2, 7.5, 12.3, 24.0, 20.2, 6.6, 0.0, 0.0, 0.5, 0.4, 1.7, 0.9, 0.0, 0.3, 0.4, 1.0, 1.2, 2.1, 6.0.
16. P. E. Belanger, W. B. Curry, R. K. Matthews, *Paleoogeogr. Paleoclimatol. Paleoeoccol.* **33**, 205 (1981); D. W. Graham, B. H. Corliss, M. L. Bender, L. D. Keigwin, *Mar. Micropaleontol.* **6**, 483 (1981).
17. High  $\delta^{13}\text{C}$  values  $>2000$  m are confirmed by data from nearby cores [C. J. Bertram, N. J. Shackleton, J. MacDonald, H. Elderfield, in *Fourth International Conference on Paleoceanography, Programs and Abstracts* (Programa Plurianual de Geologia e Geophysica Marinha, report 15, Kiel, Germany, 1992), p. 64.
18. W. B. Curry and G. P. Lohmann, *Nature* **306**, 577 (1983).
19. R. Zahn, M. Sarntheim, H. Erlenkeuser, *Paleoceanography* **2**, 543 (1987).

20. C. D. Charles and R. G. Fairbanks, *Nature* **355**, 416 (1992).
21. Percent of GNAIW =  $[(\delta^{13}\text{C}_{\text{eastern basin water}} - \delta^{13}\text{C}_{\text{SOW}})/(\delta^{13}\text{C}_{\text{GNAIW}} - \delta^{13}\text{C}_{\text{SOW}}) \times 100\%]$ .
22. W. B. Curry and G. P. Lohmann, *Paleoceanography* **5**, 487 (1990).
23. N. C. Slowey, thesis, Massachusetts Institute of Technology-Woods Hole Oceanographic Institution Joint Program (1991); \_\_\_\_\_ and W. B. Curry, *Nature* **358**, 665 (1992).
24. E. A. Boyle, in *Mesozoic and Cenozoic Oceans*, K. J. Hsü, Ed. (American Geophysical Union, Washington, DC, 1986), pp. 49-60.
25. L. D. Labeyrie *et al.*, *Quat. Sci. Rev.* **11**, 401 (1992).
26. L. L. Labeyrie and J. C. Duplessy, *Palaeogeogr. Palaeoclimatol. Palaeoecol.* **50**, 217 (1985).
27. D. W. Oppo and R. G. Fairbanks, *Paleoceanography* **4**, 333 (1989).
28. G. H. Rau, T. Takahashi, D. J. Des Marais, *Nature* **341**, 516 (1989).
29. P. S. Liss and L. Merlivat, in *The Role of Air-Sea Exchange in Geochemical Cycles*, P. Buat-Menard, Ed. (Reidel, Hingham, MA, 1986), pp. 113-127; W. S. Broecker and E. Maier-Reimer, *Global Biogeochem. Cycles* **6**, 315 (1992); W. S. Broecker, in preparation.
30. T. Veum, E. Jansen, M. Arnold, I. Bayer, J.-C. Duplessy, *Nature* **356**, 783 (1992).
31. J. C. Duplessy *et al.*, *Oceanol. Acta* **14**, 311 (1991).
32. J. Carstens and G. Wefer, in (17), p. 79.
33. A. McIntyre *et al.*, in *Investigations of Late Quaternary Paleo-Oceanography and Paleoclimatology*, R. M. Cline and J. D. Hays, Eds. (Geological Society of America, Boulder, CO, 1976), pp. 43-76; W. F. Ruddiman and A. McIntyre, *Palaeogeogr. Palaeoclimatol. Palaeoecol.* **35**, 145 (1981); L. D. Keigwin and E. A. Boyle, *ibid.* **73**, 85 (1989); T. B. Kellogg, *Boreas* **9**, 115 (1980).
34. We thank E. Joynt III, E. Franks, and N. Weicker for preparing samples and performing the analyses as well as W. Curry, C. Ravelo, and two reviewers whose comments helped clarify some ideas presented in this report. Supported by NSF grant OCE91-816259. The Lamont-Doherty Geological Observatory Deep-Sea Sample Repository is supported by NSF grant OCE91-01689 and Office of Naval Research grant N00014-90-J-1060.

4 September 1992, accepted 4 December 1992

## Order-Disorder Transition in Polycrystalline C<sub>60</sub> Films

Kelly Akers, Kejian Fu, Peng Zhang, Martin Moskovits\*

High-resolution Raman spectroscopy of polycrystalline films of C<sub>60</sub> deposited under ultrahigh-vacuum conditions show that the spectrum below 244 ± 3 kelvin consists of a superposition of two components whose relative contributions are temperature-dependent. The spectrum of the more intense of the two components is similar to that obtained for air- or oxygen-exposed samples of C<sub>60</sub> at room temperature, whereas the spectrum above 244 ± 3 kelvin corresponds to one previously reported for oxygen-free samples of C<sub>60</sub>. The results may indicate an order-disorder phase transition involving the percolation of a cluster of C<sub>60</sub> molecules engaged in coherent Raman scattering.

In 1985 Kroto *et al.* (1) proposed that carbon can exist in one of several molecular cage forms, of which C<sub>60</sub> is the most celebrated. Two years ago a facile method for the preparation of C<sub>60</sub> was discovered (2), and a large number of the molecular and materials properties of C<sub>60</sub> and substances derived from it have been determined and reported (3). In particular, the vibrational spectrum of C<sub>60</sub> has been the subject of a large number of papers in the 2 years since the discovery of the facile route for its preparation (2). Both infrared and Raman spectra (4) have been reported under a variety of conditions including high pressure (5) and low temperature (6). Despite such an extensive effort on a system that, owing to its high symmetry and the simplicity of its bonding, is vibrationally rather straightforward, the Raman spectroscopy has proven to be rather subtle.

Two distinct Raman spectra have been

attributed to solid C<sub>60</sub>. The first, reported by Bethune *et al.* (4), is an intense spectrum characterized by the appearance of the A<sub>g</sub> pentagonal pinch band at 1469 ± 1 cm<sup>-1</sup>. The same mode is observed at 1457 ± 1 cm<sup>-1</sup> in the second, weaker spectrum, reported by Duclos *et al.* (7). The center frequencies of other bands and their relative intensities also differ in the two spectra. For ease of discussion the two spectra will be referred to as the 1470 and the 1458 spectra, corresponding to the frequencies of the A<sub>g</sub> pentagonal pinch bands.

Duclos *et al.* attribute the existence of two types of Raman spectra to the fact that solid C<sub>60</sub> absorbs atmospheric oxygen. They claim that the 1470 spectrum is the oxygenated form of C<sub>60</sub> whereas the 1458 spectrum is carried by the oxygen-free variety. Oxygenation here implies an interstitial incorporation of oxygen in the C<sub>60</sub> crystal rather than chemical reaction with C<sub>60</sub>, to form, for example, the C<sub>60</sub> epoxide, as reported by Cregean *et al.* (8) or by Diederich *et al.* (9) for C<sub>70</sub>.

More recently Tolbert *et al.* (6) reported a shift in the frequency of the pentagonal

pinch mode of single-crystal C<sub>60</sub> with temperature. Although they did not indicate whether the measurements were carried out while heating or cooling the crystal, they reported a sudden increase in frequency at ~240 K, reaching a plateau at approximately ~150 K. Although these researchers were unable to record the entire spectrum, the low-temperature spectrum appears to be the 1470 spectrum and the high-temperature spectrum is the 1458 spectrum. In this report we present entire Raman spectra of C<sub>60</sub> films deposited under ultrahigh-vacuum (UHV) conditions and cycled in temperature between 55 K and room temperature.

It is known that C<sub>60</sub> undergoes a first-order phase transition at 249 K from a face-centered-cubic (fcc) structure above, to a primitive cubic structure below, this temperature (10). As this transition is approached from below, there is evidence of a "precursor state" (10) whose nature has not been clarified. Nuclear magnetic resonance (NMR) measurements (11) show a sharp break in the T<sub>1</sub> relaxation rate near 249 K, which has been interpreted as a transition between a high-temperature phase in which the C<sub>60</sub> molecules can rotate freely and a low-temperature phase in which the molecules jump-rotate between symmetry-equivalent orientations (ratchet motion). However, the molecules continue to rotate well below this temperature (12).

Purified C<sub>60</sub> samples were prepared in the now standard fashion (2) (carbon arc generation of soot followed by column chromatography). Samples were loaded into a resistively heated evaporator, outgassed before use, and sublimed onto a polished copper surface that was heatable and coolable (55 to 700 K). The entire assembly was contained in a UHV system with bottom pressures below 1 × 10<sup>-10</sup> torr. Raman spectra were collected with a SPEX (Metuchen, New Jersey) scanning double monochromator equipped with photon counting and interfaced to a personal computer. Although spectra were collected more slowly than with a multichannel system, this instrument allowed higher resolution and greater wave number accuracy.

Raman spectra obtained with the sample at 57 K, 298 K, and several intermediate temperatures are shown in Fig. 1. The spectrum obtained at the lowest temperature (spectrum B) is similar to the 1470 spectrum of Bethune *et al.* (4). The high-temperature spectrum (Fig. 1, spectrum A), on the other hand, is essentially the 1458 spectrum of Duclos *et al.* (7). The Raman cross sections of the major bands in the spectrum (compare, for example, the intensities of the pentagonal pinch modes) are some tenfold more intense in the former than in the latter. The details of the spectra obtained in the vicinity of 225 K (spectrum

Department of Chemistry and Ontario Laser and Light-wave Research Centre, University of Toronto, Toronto M5S 1A1, Canada.

\*To whom correspondence should be addressed.